NASA Contractor Report 4415

Solid Rocket Motor Witness Test

Christopher S. Welch

CONTRACT NAS1-18347
DECEMBER 1991

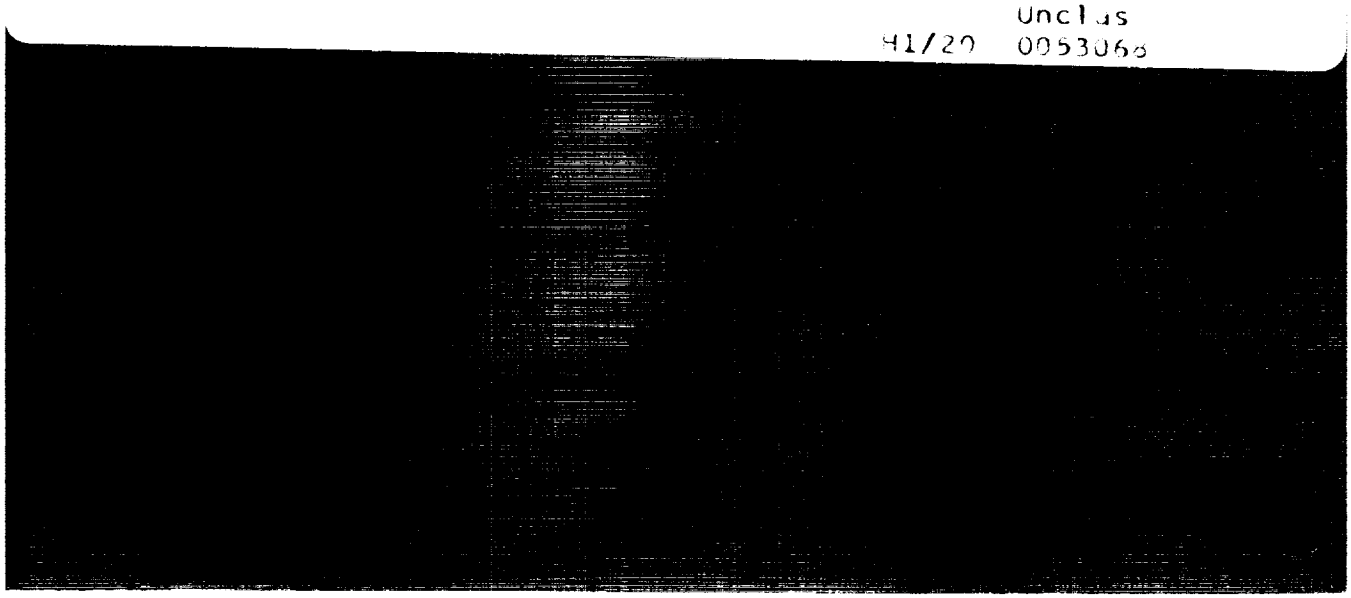

NASA Contractor Report 4415

Solid Rocket Motor Witness Test

Christopher S. Welch
The College of William and Mary
Williamsburg, Virginia

Prepared for
Langley Research Center
under Contract NAS1-18347

National Aeronautics and
Space Administration

Office of Management

Scientific and Technical
Information Program

1991

SRM Witness Test: Final Report

1. Summary of test

The Solid Rocket Motor Witness Test is an exploratory effort to identify the possible role and utility of infrared thermographic data and analysis in examining and characterizing the operation of Shuttle Solid Rocket Motors (SRM's) during static firing tests. It consisted of acquisition and analysis of infrared thermographic data from two motor tests at Thiokol[1], Inc.: the JES-3B (Joint Environment Simulator) test and the DM-9 (Development Motor) static test. During the field trips associated with the test firings, additional data were gathered from laboratory samples and test motors. Prior to this report, preliminary results and a description of the field methods were reported in "Solid Rocket Motor Witness Test: Interim Report" by the author. In addition, the laboratory tests of bondline defects were partly reported in "Numerically Enhanced Thermal Inspection of Shuttle Solid Rocket Motor Inhibitor/Liner/Fuel Bondline" by the author and T. Eden, presented at the Review of Progress in Quantitative Nondestructive Examination in La Jolla, August 1988. The main body of this report is devoted to discussing the data obtained from the DM-9 test, describing the extraction of numerical temperature data from the test, estimating parameters which describe the condition of the motor at the end of the burn, and comparing the estimates with an engineering description of the SRM given in Thiokol Report TWR-11869, "Space Shuttle Program SRM Project: Solid Propellant Rocket Motor Assembly - Disassembly Familiariztion Course" by W. E. Jones, hereafter referred to as the Jones report. Other information has come from the engineering description of the DM-9 test in Thiokol Report TWR-17371, "Space Shuttle Development Motor No. 9 (DM-9) Final Test Report", prepared by D. Garecht.

1.1 Objectives

The objectives of the SRM Witness Test were to obtain infrared image data of a solid rocket motor static test and from the data, to determine several characteristics of the motor under test. In particular, information sought was a surface temperature profile, the interior temperatures at the end of the firing, locations of any delaminations in the insulation, location of any hot gas leaks, the terminal burn pattern, and insulation thickness distribution following the test. The test was also designed to obtain a record of surface temperatures up to 500C prior to failure in the event of a catastrophic failure. As a secondary objective, data were obtained in a variety of laboratory and production settings to test the utility of

---

1. At the time of the test, the name of the company was Morton Thiokol, Inc.

thermographic nondestructive evaluation (NDE) methods in motor production and inspection.

For the secondary objective, several possibilities were identified for which thermal NDE methods could be applied to on-line motor production and inspection. Demonstrations have shown the feasibility of inspecting the case-insulation bond prior to loading a segment with propellant, of inspecting the inhibitor-liner bondline subsequent to propellant loading, and of inspecting the case-insulation bondline subsequent to propellant loading. These demonstrations have been reported previoulsy.

For the Witness Test primary objectives, it was shown in the interim report that, in the portion of the motor viewed by the imager, about 25% of the surface area, no hot gas leaks were observed and no delaminations were seen. This finding corresponds to the nominal test conditions. The remaining objectives are addressed in sections 2-5 of this report. The surface temperature image was successfully obtained over most of the period from just before the test to three hours after the test, when the motor assembly shed was repositioned over the motor. A surface temperature profile has been constructed from this data. Furthermore estimates from the data have been made for both the terminal burn pattern and the remaining insulation thickness. These estimates show the feasibility of remote infrared image data for determination of these parameters. The only objective which was not attained was to determine the temperature pattern inside the motor at the termination of the burn. The difficulty in determining this temperature pattern is discussed in Section 3.1 of this report.

1.2 Field work

The field work took place during two visits to Thiokol, Inc. during the months of November and December 1987. These visits were scheduled to cover the JES-3B and DM-9 tests, respectively. Particulars of the tests, the equipment and the experimental protocol are contained in the Interim Report, which also includes the complete analysis of the JES-3B data.

Some aspects of the experiment are repeated here because they shed light on the resulting data and the methods used to extract numerical estimates. The nature of the test is such that safety required the IR imager to be unattended during the burn and some time thereafter, while toxic concentrations of combustion products dissipated. In practice, the imager was unattended from about 30 minutes prior to ignition to about 30 minutes following ignition. The imager settings prior to ignition were chosen to have as large a maximum temperature as possible, as the actual maximum expected temperature was not known yet. On regaining access to the equipment following the burns, the imager was reset to a more sensitive scale

to use as much of the dynamic range as possible under the assumption that maximum temperatures would not exceed temperatures in evidence at that time. In the DM-9 static test, there was also a power loss to the imager subsequent to the firing, so data were lost for an uncertain amount of time. Thus, the image data consist of two segments, each of which has a different scale, level reference, and time reference. Part of the data extraction effort was to reconcile the references for the two segments.

The DM-9 test was performed during mid and late afternoon on December 23, 1987, with ignition at 2:50 pm. The air temperature was below freezing, and the ground was mostly covered by snow. The sky was overcast with occasional light snow flurries, and a steady wind blew from the north at an estimated 20 mph. The snow was never heavy enough to hamper visibility between the imager and the motor.

2. Data extraction

The objective of data extraction was to obtain temperature time series at representative locations on the SRM. The process is in many ways complementary to the usual procedure for obtaining temperature patterns using point sensors. With point sensors, an array of sensor locations is chosen, individually calibrated sensors are mounted at the points, temperature data are obtained from the sensors, and spatial temperature distributions are inferred over the entire SRM by making judicious use of interpolation schemes to fill in between the point data. When the sensor array is designed, a decision is required about the expected distribution pattern, and the possibility is accepted that a small temperature feature will miss the sensor net or be unduly weighted by falling on a sensor. With image data, the entire image is scanned with a single calibration and a fixed spatial resolution, so the response of the image to any sub-resolution features is uniform over the image. Then, locations which are representative of the spatial pattern apparent in the image are chosen to extract temperature data at particular points, synthesizing the records obtainable from point sensors.

The data extraction process for the point data synthesis covers the steps which convert the data from VCR tape information to tables of values as a function of time. These steps include assignment of times to the video frames, averaging of frames to produce image data "snapshots" over fixed periods at nominal times, reconciliation of nominal times with actual times, extraction of numerical gray level values, and assignment of temperature zeroes and scales to the gray levels.

2.1 Rerecording and frame time assignment

The first step for the DM-9 data was to rerecord the video cas-

sette data on an AMPEX VTR 80 Video Tape Recorder (VTR) equipped with a TBC 80 Time Base Corrector. The VTR labels each incoming video frame with a sequential label which also denotes the nominal time in hours, minutes, seconds, and frames, there being 30 frames in a second. For later reference, each frame may be addressed repeatably by using its unique time label. In analysis of the tape, the first stable frame was labeled as zero time, so a local time frame was established with a precision of 1/30 second. This time label for each frame may be superimposed on the video image, permitting an easily interpreted label to be included on each image produced during analysis.

The rerecording process for DM-9 was started at about 7 minutes before ignition. The ignition event is on the frame labeled 0:07:16:16, denoting 0 hours, 7 minutes, 16 seconds and 16 frames (or 16/30 second). The ignition event further serves as a redundant time reference point for verifying tape position and counter setting for a given tape mount. Times prior to the power loss event are thus referred to the ignition time, the time of greatest physical significance, with a precision of .03 seconds. The power loss occurred after the frame labeled 0:29:04:09, so the good time reference was available for 0:21:47:23 following ignition. The duration of the power loss is estimated at 13 minutes, with an uncertainty of 1 minute. After power was restored, the scale was reset along with the threshold level of the imager, a procedure which took an additional 0:01:22:28. The result is that the data frames show a drop-out of about 16 minutes, covering the power loss and the subsequent adjustment period, and the times after the drop-out have a systematic uncertainty on the order of one minute with respect to those prior to the drop-out. The frames following the drop-out have good relative times among themselves. The temperature reference is likewise consistent among the frames prior to and subsequent to the drop-out, but there is an unknown shift during the drop-out.The nominal sensitivity before the drop-out was 500 C full scale, while after the drop-out it was 20 C full scales. In subsequent processing, the nominal values were considered actual values. Because of the great difference in sensitivity, the frames before the drop-out, which shall be called the early frames, were treated differently than those after the drop-out, or the late frames.

2.2 Image production

For the data reported here, the steps of image production and numerical value data extraction are different from the ones described in the Interim Report. This is because new equipment became available since that time which permitted digitization and storage of up to 32 sequential full frames during a single pass of the video tape.

For the early frames, data were captured over three sequential

seconds, one second (32 frames) at a time. Synchronization was accomplished by watching the time marker in the image and pushing the "RETURN" key on a computer keyboard when the appropriate nominal time was displayed. Repeated captures showed that, with a little practice, this procedure introduces a delay of 7 frames from the nominal times with an uncertainty of plus or minus two frames. The captured frames were then moved into a buffer with larger dynamic range in the computer and averaged. With approximately 92 independent frames included in each average, the gray value noise level is reduced by a factor of about 9.6. The noise level for the data in the early frames is dominated by the least count of the internal digitizer, which produces a least count level shift of just under 2C on the 500 degree full scale sensitivity setting. With the reduction, the random component is reduced to 0.2C. Unfortunately, at the low levels of contrast used in the early frames, the noise was dominated by non-random digitizer "pattern" noise at the level of about 1.0C, half the least count level. The early frames are thus self-consistent to about 1C. They were captured at one or two minute increments after the beginning of firing.

For the later frames, the relation between the least count noise and the random noise from the imager was reversed. Here, the imager noise is 0.15C, according to the manufacturer, while the least count level is .08C. If the limiting pattern noise is at half the least count level as it was for the early frames, about one quarter of the random noise level, then an average of 16 frames will reduce the random noise to the level of the pattern noise. An average of 32 frames leaves the pattern noise dominant. Because 32 sequential frames can be captured by the digitizer at one time, it was possible to capture the later frames in an automated manner. For these frames, the tape recorder was run nonsynchronously with the computer, which was controlled by a command language script. The tape time was displayed on the image, and so captured with the 32 sequential frames. The resulting run produced averages of 32 frames, about 1 second, at intervals which turned out to be uniformly spaced at 5 minutes. Examination of the data shows that the pattern noise is again limiting and, at approximately 0.1 C, consistent with the estimate.

The resulting set of images comprises 13 early frames and 11 later frames. These frames are separate from the ones used in the Interim Report, although they come from the same rerecorded magnetic tape. An example of one of the frames was shown in the interim report as Fig. 4.4 and is repeated here as Fig. 2.1. Motor images from these frames are collected in Figure 2.2. To produce this figure, the data from the split frame format were numerically processed to "reassemble" the rocket and are presented from top to bottom as a time sequence. Only the late frames are shown in the figure, for the high gain setting of the early frames produced imager artifacts which

ORIGINAL PAGE
BLACK AND WHITE PHOTOGRAPH

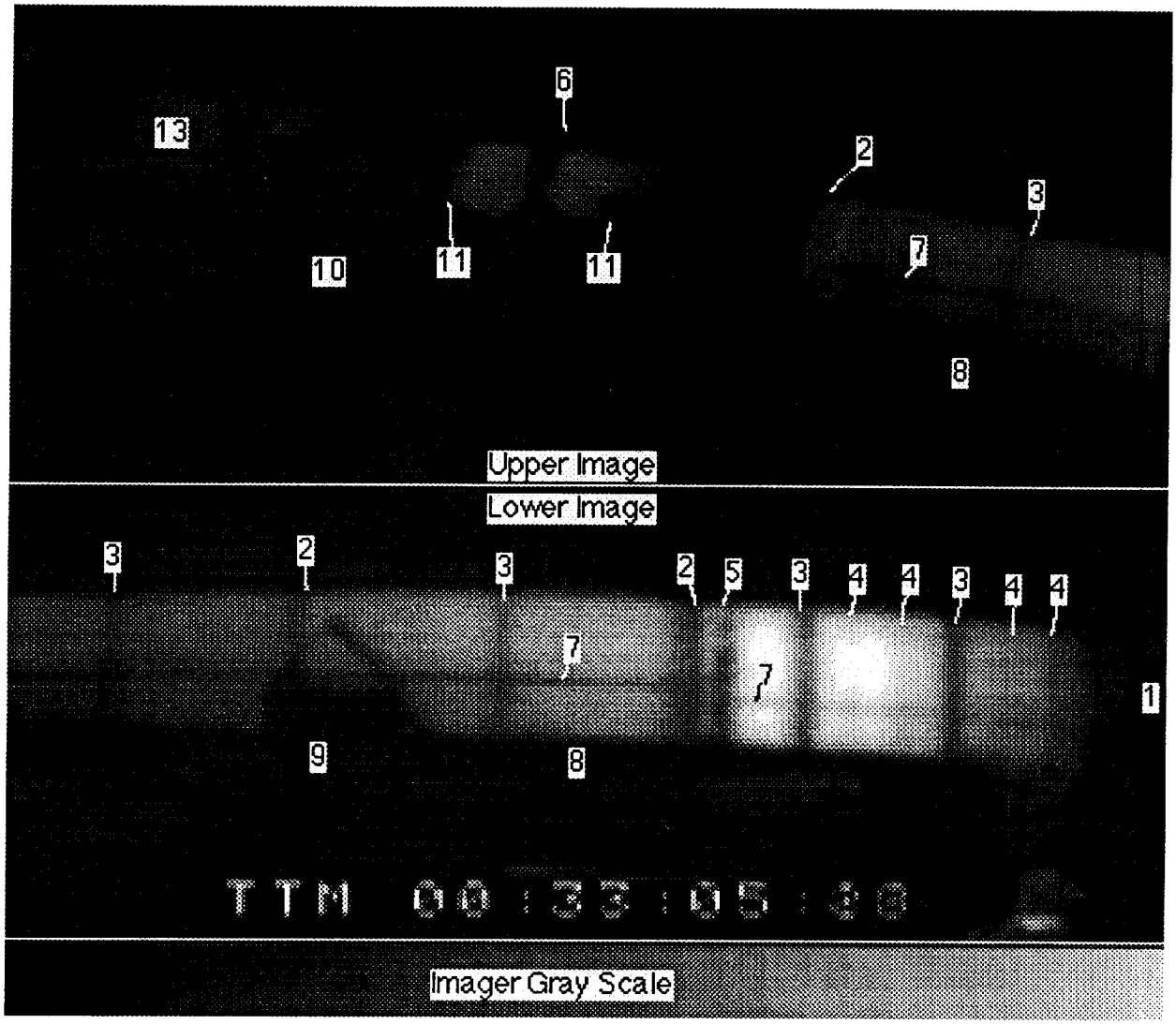

Figure 2.1. Infrared image of a Space Shuttle solid rocket motor after static test DM-9. Numbers refer to notes following.

Notes for Figure 2.1

Item	Description
1.	Nozzle. This shroud hides the thermal radiation from the forward nozzle area from the imager. The aft nozzle area was intentionally cropped from the image to prevent possible saturation from the flare during the firing itself.
2.	Field joint. The slight thermal contrast adjacent to these joints may carry information about insulation remaining following the test.
3.	Factory joint

Notes for Figure 2.1 - Continued

Item	Description
4	Stiffener ring. These rings are installed on the aft section only.
5	External Tank (ET) attach ring. This ring is associated with the aft motor support for the test.
6	Forward motor support for the experiment.
7	Systems tunnel. The insulation covering this tunnelis both cooler than the motor in general and has a different emissivity. It produces a cool line in the image.
8	Instrument wire cable. This cable, which carries many wires associated with test measurements, blocks the direct view of much of the bottom of the motor from this vantage point.
9	Wooden shelter. This housing stands about half way from the imager vantage point to the motor.
10	Mound of dirt. This mound blocked the view of about half of the forward segment of the motor.
11	Other instrumentation. Several other instruments, perhaps cameras, were mounted close to the motor on the mound labeled 10.
12	Ghost of imager temperature range selector. Part of the temperature range selector indication, which occupies part of the left side of the original image, is visible on the right side. This indication stands for the 20 degree C range setting. (Note: This feature is not seen in Figure 2.1)
13.	Concrete Reaction Mass

appear as a spatial pattern which gives the image a "double-exposure" quality in comparison with the later frames.

Examining the images rather than the artifacts, a general pattern of heating and cooling emerges. The thermal pattern appears segmented, with definite cool places appearing in circumferential bands which correspond to the joints and stiffeners of the motor. The forward segment divides into two distinct halves, with the forward part heating quickly and cooling gradually, while the aft part of the forward segment heats quickly and then cools quickly. The center and aft segments have a similar heating and cooling pattern pass through

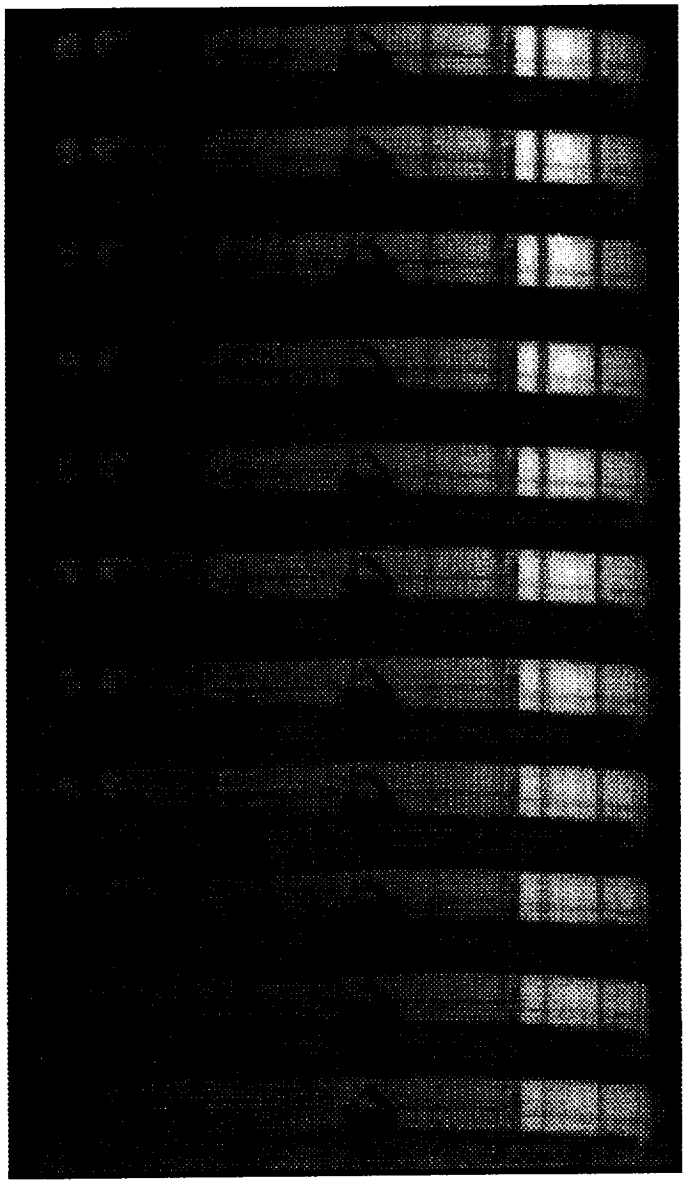

Figure 2.2. Sequential montage of "late time" motor images used in the analysis. The images were assembled numerically from split frame data similar to Figure 2.1. Times annotated in the images are frame times, for which ignition was at about 7 minutes.

them. The maximum temperature and the time to reach maximum temperature increase as one progresses aft from the fwd-ctr segment to the center of the aft-ctr segment. From there to the back of the motor, the peak temperature declines, but the time to the peak continues to increase. In contrast to this axial pattern, the circumferential variation is much smaller except for a cool line caused by an external wiring harness and the systems tunnel of the motor. Thus, it is reasonable to describe the temporal temperature variation of the motor by obtaining point measurements at each of the segment centers,

corresponding nearly to the temperature maxima in each segment, as a function of time.

2.3 Numerical value extraction

At this point, a set of pattern-noise limited images has been obtained for two sets of frames. The frame sets have different zeroes and different gains. The imager was not moved during the data run, so all of the images are viewing the same scene. The next objective is to extract temperature data corresponding to the segment centers on the image in each of the frames. As a first step, it is useful to estimate the area which acts as a "point" on the image.

Each digitized frame is represented by a two-dimensional array of points with 512 points in each direction. According to manufacturer's specifications, an imager frame has 150 resolvable points per line and 200 resolvable lines per frame. This is consistent with the measurements obtained in our laboratory. The portion of the motor in the lower image is about 85 feet long, so the resolution is about 85/150 feet, or 7 inches. To achieve accurate temperature readings, the imager manufacturer recommends a spot diameter of at least 5 resolution elements, or about 35 inches. This size is larger than the joint areas, so while the joints are well located in the image as cool lines, the imaged temperatures at the joints are not expected to be accurate. On the other hand, the temperatures in the middle of the segments should be representative.

To examine this representativeness, a line of data points was obtained from a transverse scan of the motor cross-section on the aft part of the center-aft segment. This segment and image were chosen as having a clear view of a region with substantial temperature elevation and little possibility of detector saturation. It should ideally produce a square "top hat" response. The line data, shown in Figure 2.3, show a central region of elevated temperature, with the bottom of the motor corresponding to the left side of the graph. The data deviate from the boxcar ideal in several ways. The step-like appearance of the graph is a result of oversampling the image to produce the graph. Each step corresponds to a pixel, and four steps to an Instantaneous Field of View (IFOV) according to the imager specifications. The minimum in the center of the graph corresponds to the cool systems tunnel, which is located half-way up the viewed side of the motor. It plausibly is the response to a very small cool target. Thus, it can be taken to express the vertical part of the spatial response function of the camera system, except that the baseline is not well defined. Similarly, the left hand edge of the temperature elevation corresponds to the masking of the lower part of the motor by the wire harness. The right hand edge, corresponding to the tangent view of the top of the motor, can decrease for two reasons. First is the response function of the system and second is the non-

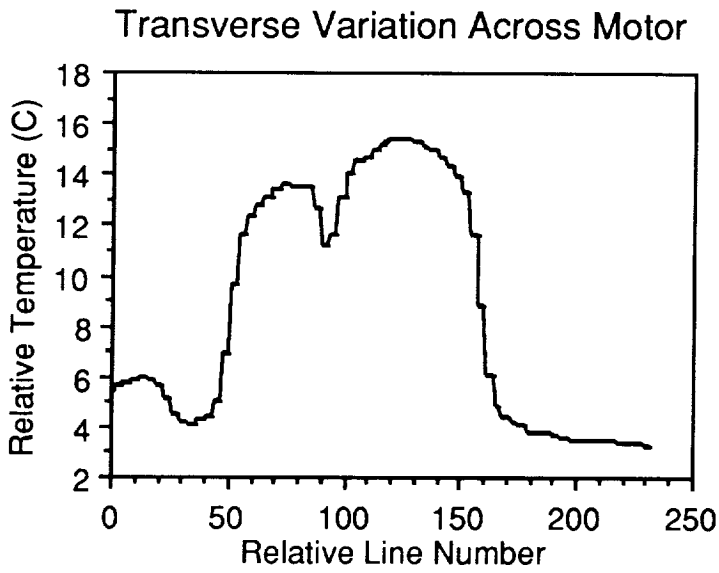

Figure 2.3. Temperature pattern across a transverse section of the motor showing the combined effects of actual temperature variation, non-Lambertian emissivity response at grazing angles and instrument spatial response.

Lambertian response of emission at nearly-grazing angles of view. Such deviations are expected to be significant only for viewing angles greater than 60 degrees to normal, corresponding to only 10 units on the horizontal scale of the graph. The similarity of response between the right and left edges suggests that non-Lambertian response is not an important consideration in this data. The manufacturer requires a size of 5 IFOV's to acquire an accurate temperature. This corresponds to 66 counts on the x axis to obtain an accurate temperature. Thus, the narrow plateau between the system tunnel and the edge of the motor represents the region of accurate response. The lower temperature maximum value below the systems tunnel may be attributed to failure to obtain a full 5 IFOV's of clear area rather than an actually lower temperature. To get good estimates of the temperature of each motor segment, then, it is necessary to sample the data from the portion of each segment in the middle of the clear space between the systems tunnel and the top edge of the SRM.

To bring the data from the two sets of frames into parity, the apparent temperature from the reaction mass is used as a reference, under the assumption that the reaction mass changed its temperature relatively slowly during the data acquisition time. Because the reaction mass was sheltered in the moveable building until the morning of the test, the temperature of the reaction mass cannot be considered to be the ambient air temperature. Thus, the resulting relative temperatures are consistent between frame sets, but the zero of the scale does not represent a thermal equilibrium. The scale change

between the frame sets was assumed to correspond with the nominal scale ranges for each setting, *i.e.* 500 C full scale in the early images and 20 C full scale in the later images. Emissivity was not considered in the data reduction, so it is assigned a value of 1.0. The calculated relative temperatures are thus uniformly low by perhaps 15 percent. At this point, no need for emissivity estimates has arisen, and the biased temperatures seem quite serviceable.

An inspection of the split-image format of the data identifies 17 locations which correspond to the center portions of a given segment or the reaction mass. The motor locations are distributed as follows: three on the forward segment, four on the forward-center segment, two on the aft-center segment and seven on the aft segment. As the segments are each composed of a series of cases separated by factory joints, each case produces its own temperature maximum. In addition, the image of the forward segment is split into two parts by a test stand support, and the aft segment image is similarly divided by stiffener rings. The locations of the temperature maxima are summarized in Table 2.1 and Fig. 2.4. The motor firing in the

Table 2.1. Locations at which time series data were extracted from thermal images of test DM-9 of the Shuttle Solid Rocket Motor.

Point	Description	Sub-Image	Pixel	Line
1	Longitudinal Face, Reaction Mass	top	142	390
2	Fwd Segment, Fwd Case, Fwd part	top	28	368
3	Fwd Segment, Fwd Case, Aft part	top	264	366
4	Fwd Segment, Aft Case	top	316	356
5	Fwd-Ctr Segment, Fwd Case	top	402	330
6	Fwd-Ctr Segment, Aft Case	top	480	324
7	Fwd-Ctr Segment, Fwd Case	bottom	24	172
8	Fwd-Ctr Segment, Aft Case	bottom	104	174
9	Aft-Ctr Segment, Fwd Case	bottom	190	174
10	Aft-Ctr Segment, Aft Case	bottom	268	172
11	Aft Segment, Fwd Case	bottom	342	162
12	Aft Segment, Ctr Case, Fwd part	bottom	372	160
13	Aft Segment, Ctr Case, Ctr part	bottom	391	160
14	Aft Segment, Ctr Case, Aft part	bottom	409	160
15	Aft Segment, Aft Case, Fwd part	bottom	433	158
16	Aft Segment, Aft Case, Ctr part	bottom	450	158
17	Aft Segment, Aft Case, Aft part	bottom	470	156
18	Low Grey Bar*		1	20
19	High Grey Bar*		512	20
20	Top of Screen Black*		234	448
21	Top of Screen White*		234	468

* These locations are not indicated on Figure 2.4, which has been cropped for display.

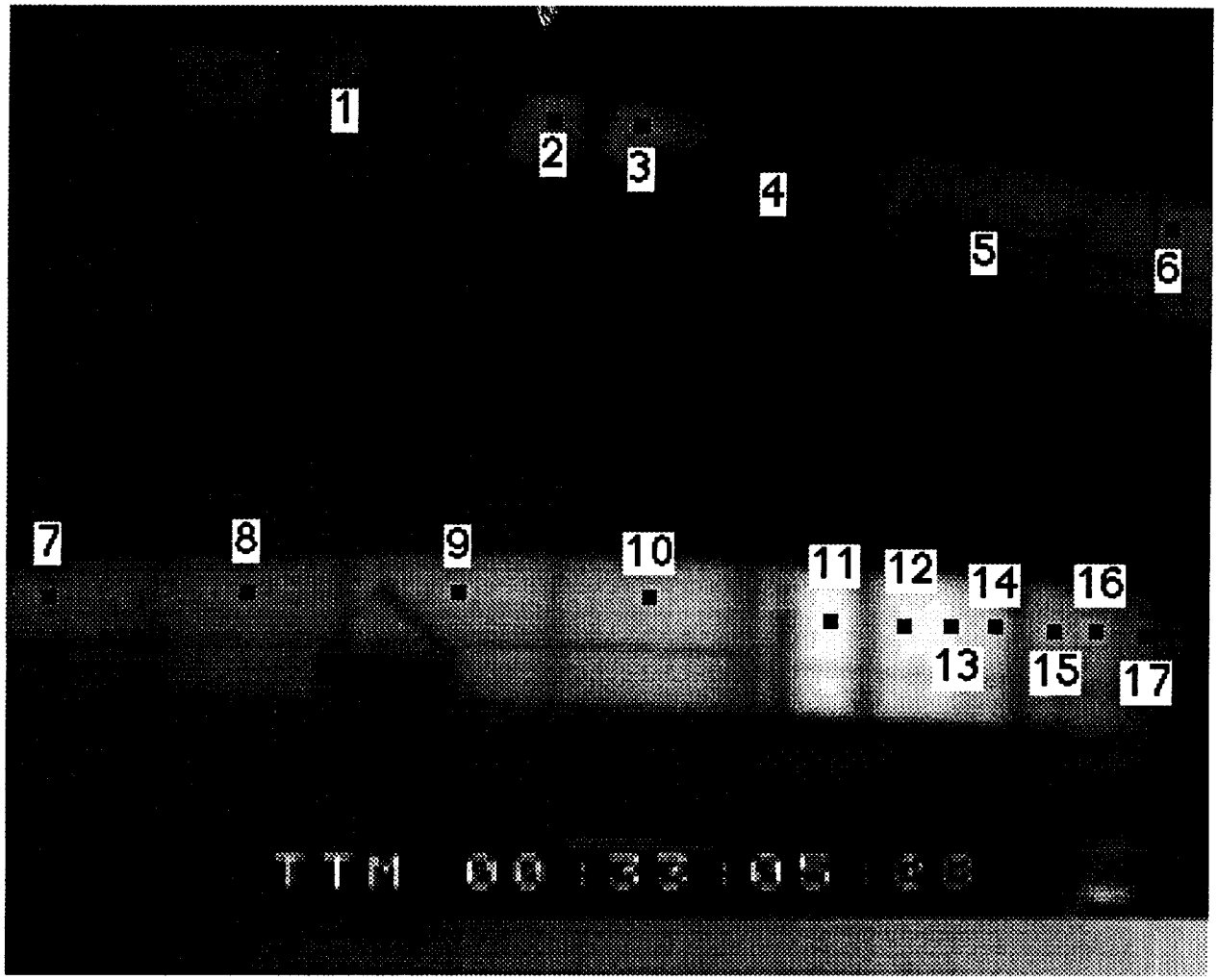

Figure 2.4. Locations of points on the thermal images of Shuttle Solid Rocket Motor test DM-9 at which representative time series of temperature were extracted.

data time scale occurred between 436 seconds and 556 seconds. The images taken during this period were found to be excessively noisy either because of imager response to the sound field or because of unresolvable reflections of radiation from the exhaust flare. The time series obtained from the remaining images are expressed as temperature relative to the reaction mass as a function of time in Fig. 2.5-2.8. Each of these figures represents one of the four motor segments, the figures progressing from forward to aft. Figs. 2.5, 2.6 and 2.8 are subdivided into a and b parts, the b part being a magnification of the early data for clarity of the early response. That each segment has its own temperature cycle is suggested by the difference in temperature scales in each of the figures.

In Fig. 2.6, depicting the center-forward segment, the data were taken from both the top and bottom halves of the image, the center-forward segment corresponding with the image overlap region.

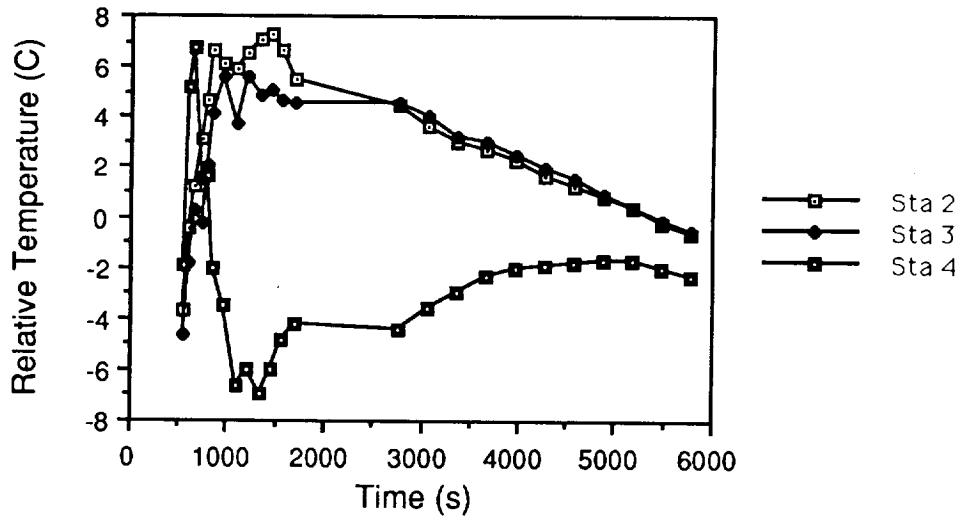

Figure 2.5a. Temperature records extracted from the forward segment of the Shuttle Solid Rocket Motor during test DM-9. Burning occurred between 436 s and 556 s.

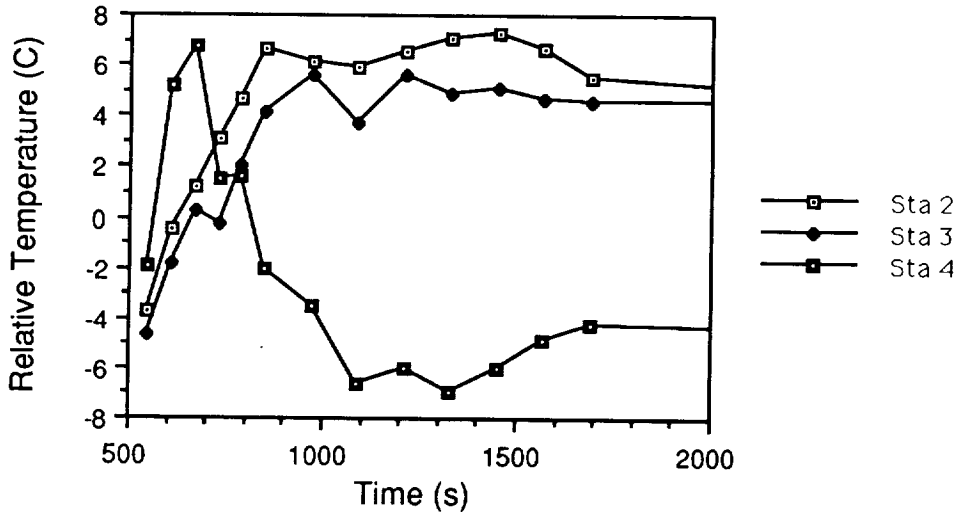

Figure 2.5b. Magnification of the early part of the temperature record in Figure 2.5a.

The two data sets should then be duplicates, differences indicating primarily system-induced variations. In Figure 2.6, the agreement is not good between the duplicate samples in the forward part of the segment, diverging by as much as 8 degrees in the early frames and by a consistent 1 degree in the later frames. In contrast to this, the data for the aft part agrees within 1 degree in the early frames and within about 0.2 degrees in the later frames. The question arises why the discrepancy? If the data are simply poor, why is one set of errors so much different from the others? A closer examination of the differences between Stations 5 and 7 shows them to consist mostly of two offsets, one applying to the early frame data and the other to the late frame data. Except for these offsets, the data track as well as those from Stations 6 and 8. An examination of the data provides

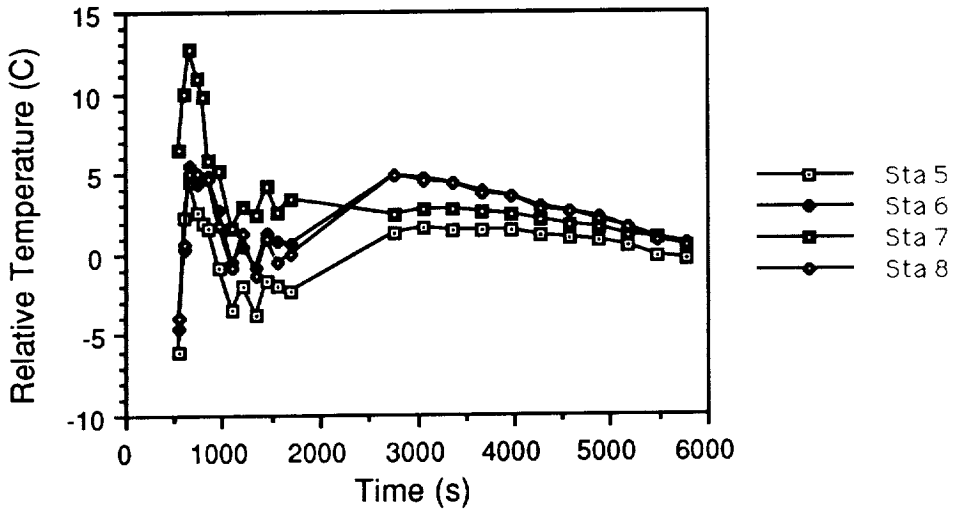

Figure 2.6a. Temperature records extracted from the center-forward Shuttle Solid Rocket Motor Segment during static test DM-9. Burning occurred between 436 and 556 s.

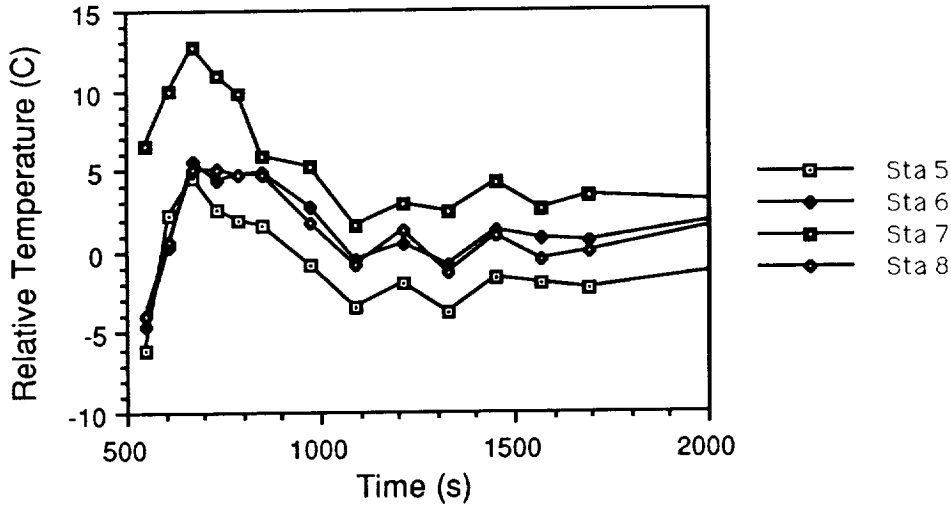

Figure 2.6b. Magnification of the early part of the temperature record in 2.6a.

the answer. The lower image point is located close to the left-hand edge of the image, and there is a "shadow" of the imager-generated marking along the left side of the image which indicates the setting of the "scale" control. This shadow adds a constant bias value of brightness to the data in the lower image. This constant value is different for the images taken at different sensitivities, and so for the early and late images. The agreement between Stations 6 and 8 thus is more representative of actual variations due to the imaging process between essentially identical samples. These variations indicate the system noise including the imager, the various tape recorders and the digitizer for the image processor. Fig. 2.9 shows the difference between the values at station 6 and 8 to illustrate

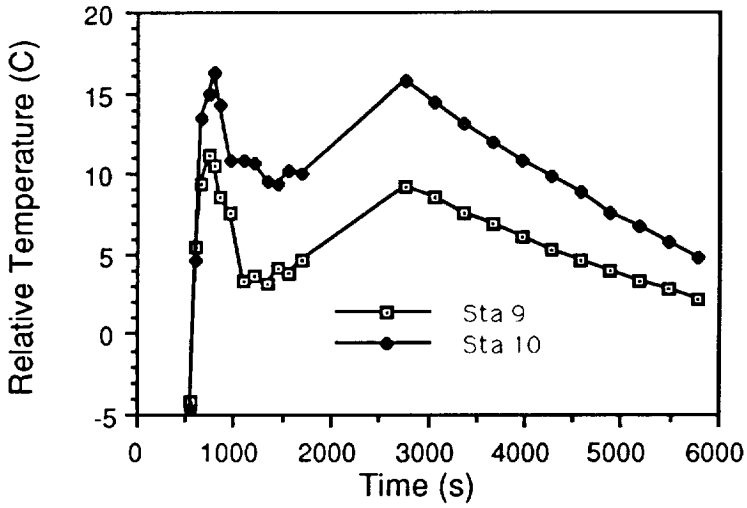

Figure 2.7. Temperature records extracted from the center-aft Shuttle Solid Rocket Motor Segment during static test DM-9. Burning occurred between 436 s and 556 s.

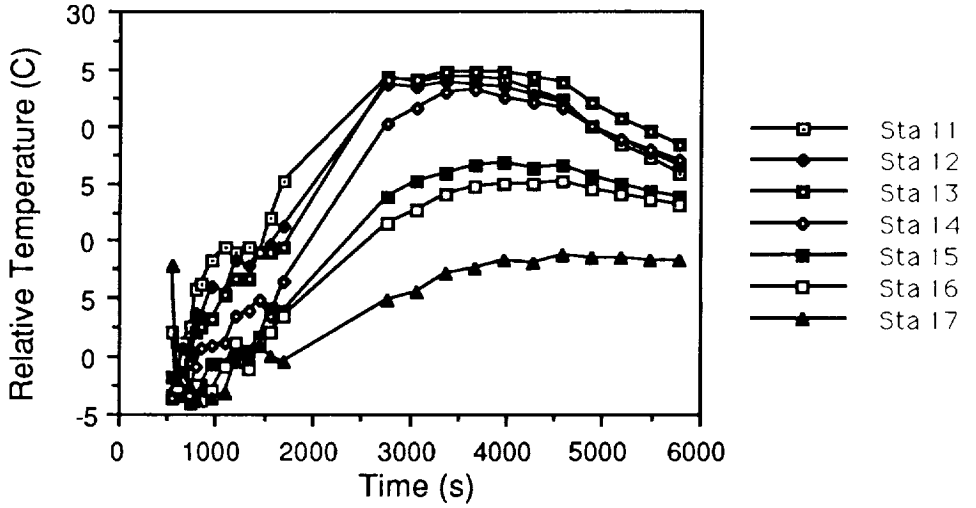

Figure 2.8a. Temperature records extracted from the aft Shuttle Solid Rocket Motor Segment during static test DM-9. Burning occurred between 436 s and 556 s.

the system noise. In particular, the differences between the early frames and the later frames are apparent.

As the discrepancy in Station 7 is related to the edge of the image, it only affects that station, so the remainder of the figures can be taken to be representative of the temperature variation of the part of the image they are taken from, save for emissivity corrections. The emissivity corrections should be the same for all the case segments, as they are painted with the same kind of paint. The data all show the same general qualitative shape in time, with a rapid initial heating followed by a gradual cooling back towards ambient. In addition to this overall pattern, the data between the

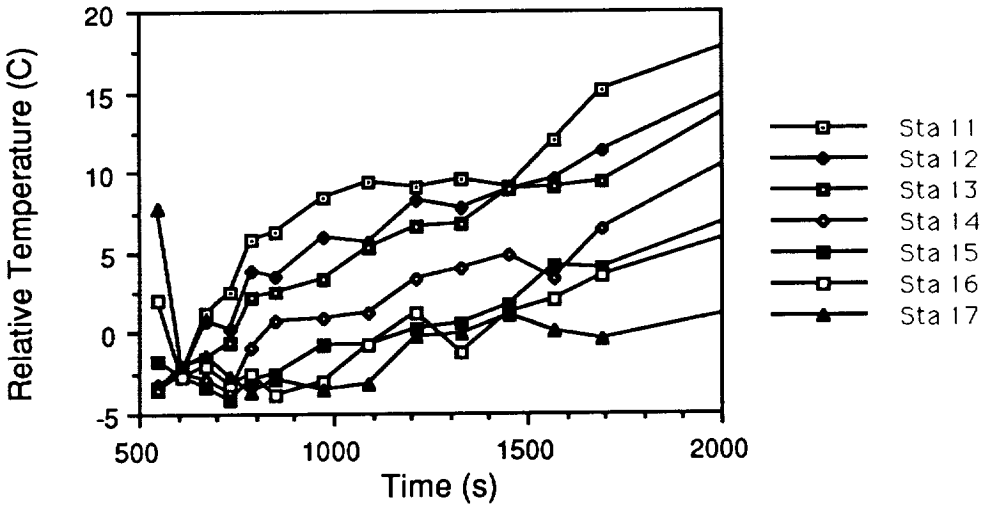

Figure 2.8b. Magnification of the early part of the temperature record in 2.8a.

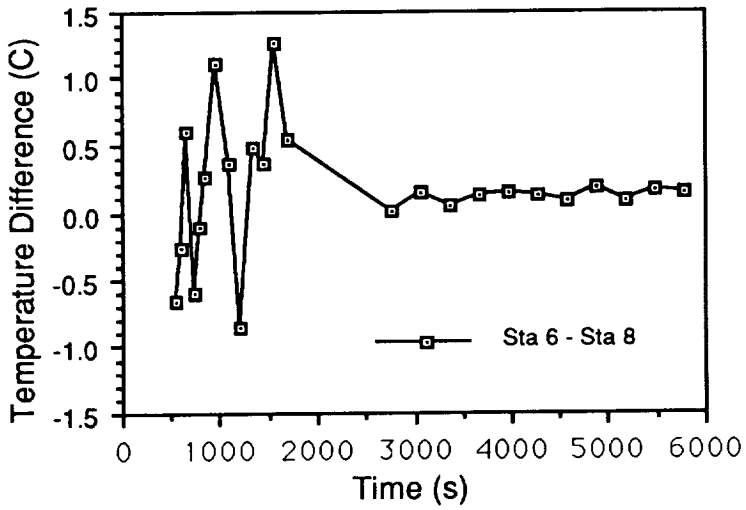

Figure 2.9. Difference between temperature values extracted at stations 6 and 8. Because these stations represent the same point on the motor, the difference provides an estimate of the random errors in the extracted temperature values.

aft part of the forward segment and the forward part of the aft segment show an intermediate cooling event with a peak value of about -13 C at the forward occurrence and diminishing and peaking later as the data move aft. A summary of characteristics of the observed heating and cooling curves for the motor is given in Table 2.2. It is this qualitative shape which must first be described by any model from which parameters might be estimated. If the heating is taken as the signature of the firing itself, the cooling is plausibly associated with the fire extinguishing process done immediately after the firing by flushing the motor with carbon dioxide to preserve its state at the end of the firing. In shuttle operations,

Table 2.2. Selected characteristics of time series data from Solid Rocket Motor test DM-9_

Station	x location (inches)	Maximum Temperature (C)	Time of Max T after burn(s)	Maximum Cooling (C)
2	586	6.9	894	0.7
3	639	5.3	414	1.7
4	771	6.5	114	13.2
5/7	931	4.5	114	7.9
6/8	1091	5.5	54	6.1
9	1251	10.5	174	7.6
10	1411	15.2	234	6.3
11	1534	24.3	2808	0.5
12	1597	23.5	2808	0.5
13	1637	24.7	3107	0.0
14	1677	23.0	2808	1.1
15	1717	16.8	3413	0.5
16	1757	15.0	4011	2.0
17	1797	8.6	4011	2.2

the fires are extinguished by being exposed to the vacuum of near space, according to the Jones report.

3. Model Formulation

The method of inferring aspects of the state of the interior of the rocket motor from the temperature record of the motor surface involves the use of a physically realistic model. The model incorporates what are judged to be the most important factors involved and produces a temperature record, which is then compared with the observed temperature record. Some of the parameters used in the model, such as the thickness of the steel shell, are well known, while others, such as the motor temperature at the end of firing, are relatively unknown. The unknown parameters are varied until the modeled temperature record corresponds closely with the observations. The values of the unknown parameters then become the model estimates of the unknowns. The model is then operated by giving the parameters small variations around the values of the fit to examine the sensitivity of the calculated temperature to variations in the parameters. Where the sensitivity is small, the estimates of the associated parameters are correspondingly inaccurate. Particular care needs to be taken to identify combinations of parameter changes having equal and opposite changes on the temperature record, for when such cases exist, a good fit of the model to the data does not determine values of the parameters, but only establishes relations between acceptable value pairs of the opposing parameters.

3.1 Qualitative physical description

The physical model is based on a description of the process by which heat is generated and transferred to the observed surface. The process used in this study is that, during the last few seconds of burning, the insulation is exposed to the hot gasses generated from still-burning sections of the motor. The time of initial exposure is determined mostly by the time elapsed between local burn-out and final burn-out. This exposure changes the phase of some of the insulation layer and removes some by ablation. At burnout, the exposed insulation surface is heated to incandescent temperatures, and the dominant mode of heat transfer within the motor is radiation. This high temperature exchange of radiant energy will tend to bring the entire exposed surface to the same temperature, which is rapidly decreasing because of radiation escaping through the nozzle. This thermal balance dominates the cooling of the motor until the temperature has fallen so low that radiant exchange is no longer dominant. At this time, only a few seconds after the burn, a certain amount of heat has been trapped in the insulation, and it is this heat which passes through the remainder of the insulation and the steel skin to be observed on the outside surface of the motor. An unfortunate consequence of this sequence of events is that the value of the initial temperature within the motor following burnout is not able to be determined accurately from the temperature evolution of the skin, because much of the heat which was represented by the initial temperature escapes the system as radiation through the nozzle without affecting the observed surface temperature distribution. During the non-radiative part of the cooling, the inner layer of charred insulation, which had been in close mutual thermal contact by virtue of radiant heat exchange, becomes connected only by the much less effective mechanism of mutual contact with the remaining gas in the motor which circulates by natural convection. As will be shown below, thermal conduction through the motor skin is even less effective during this part of the cooling owing mostly to the size of the motor and the resolution scale of the image data.

3.2 Reduction to one dimension

A great simplification in the thermal analysis is made by approximating the thermal propagation from the inner part of the rocket to the outer surface, where heat is observed, by a collection of one-dimensional problems rather than the three-dimensional problem it actually is. This simplification is achieved by demonstrating that the temperature observed at any point on the rocket surface is associated primarily by the heat injected into the insulation directly opposite to that surface and not to heat injected into adjacent locations. Because the heat transport through the insulation

and from the adjacent regions is through conduction, it suffices to compare the characteristic times for the two transports. For the through-insulation transfer, a characteristic time can be estimated by noting that it takes up to 3000 seconds after ignition for the temperature to peak on the surface, in many cases the time being much less. To estimate the time for heat to reach a point from an adjacent point, the assumption is made that it travels through the steel part of the skin, rather than the insulation, and so has a characteristic time of L2/k, where k is the diffusivity of the D6AC steel used in the motor and L is about 4 feet, the size, on the motor surface, of a thermal feature required to obtain an accurate temperature value. evaluates to about 40 hours. The duration of the data run was about 4 hours. This time is too short for significant heat to transfer from adjacent locations by diffusing through the steel skin. There is some experimental evidence to support this conclusion. During the latest part of the data run, a warm temperature fringe is observed at the lowest part of the aft portion of the motor. This fringe is attributed to the cooling water (~40F) which was sprayed onto the underside of the motor by a deluge water spray system in order to prevent overheating from a puddle of aluminum slag which forms during horizontal static firings. It is only towards the end of the data run that the heat from the deluge system is visible above the wiring harness. Thus, both theoretical and experimental considerations support reduction of the heat transfer problem to one dimension for the interpretation of thermographic data. For this purpose, individual one-dimensional models need be generated only for those points at which verification temperature records are extracted.

3.3 Model formulation

The numerical model package used to formulate the one-dimensional model for the Witness Test results was TOPAZ2D, a 2-dimensional finite element code developed at Lawrence Livermore Laboratories. The actual elements used were rectangular, and the model geometry consisted of a line of these elements. All of the elements were chosen to have the same size, and 60 or 100 elements were used to span the thickness of the motor casing, liner, insulation and char. One advantage of the one-dimensional model is the resolution attainable. The thickness of an individual model element is only 0.25 mm, yet the entire model comprises only 122 or 202 nodes. The painted surface is considered to have negligible thickness; the steel casing takes 49 elements; the liner, one element, and the insulation, 10 or 50 elements. Of the insulation elements, some number were chosen to have been converted into a glowing "char" layer, while the remainder were chosen to be cool for initial conditions, which were taken to be at the moment of burnout. The heat resident in the char layer was the forcing heat in the model. The cooling from the CO_2 injection

following the burn was not modeled. The cooling in the model was chosen to be radiation cooling the char layer, with the radiation escaping through the nozzle to a sink at 273K, and forced convection cooling at the outside of the motor where it was exposed to the wind, also at 273K.

3.3 Numerical values of model parameters

The geometry of the model was taken to represent a section through the solid rocket motor which is not near a joint, the so-called "acreage part". It has a steel section of thickness 0.49 inches (1.25 cm) followed by liner material of 0.01 in (0.025 cm). Inside is NBR covered with a char layer, which is assumed to have been ablated to some extent. The NBR and the char layer have either of two total thicknesses, 0.1 inches (0.25 cm) or 0.5 inches (1.25 cm). This can be compared to a range in the SRM of between 0.03 inches (.076 cm) and 1.45 inches (3.68 cm) [values from the Jones report]. The steel has a density of 7830 Kg/m3, a thermal conductivity of 37.4 Watts/(m-K) and a heat capacity of 460 J/(Kg-K). The liner has corresponding values of 983 Kg/m3, 0.185 W/(m-K) and 1963 J/(Kg-K), and the NBR has values of 1290 Kg/m3, 0.268 W/(m-K) and 1590 J/(Kg-K).

The character of the char layer is most uncertain. In the physical formulation, the char layer is initially heated to 3600C. The properties of an ablated char layer are not so firmly documented as those of the parent material, so estimates were made. These were a density of 860 Kg/m3, 2/3 of the insulation density, a conductivity of 4.0 W/(m-K) and a heat capacity of 840 J/(Kg-K). The char approximation was made using the assumption that charred material will consist partly of charcoal or amorphous carbon, but that it will be highly fractured, so its effective density is about half of amorphous carbon. On the other hand, for the first pass, its specific heat was given a constant value about twice the room temperature value of carbon to account for the increase in heat capacity of carbon with temperature over the temperature excursion of the char. In a similar vein, the thermal conductivity of the char layer was set approximately to that for amorphous carbon, which is seen to be much higher than the insulation yet much lower than the steel.

The heat transfer coefficient for the surface to the atmosphere was taken as 9.2 W/(m2-K). This value was taken to fit the long term observed temperature decay, as shown in the next section. In comparison with other values, it is higher than the value given by Carslaw and Jaeger [Eq. I(6)] for long cylinders in a steady flow, which, with a wind speed of 20 mph gives 5.23W/(m2-K), yet smaller than the value measured in our laboratory tests with 1 square foot SRM samples of 15.48 W/(m2-K) [W. Winfree, pers. comm.]. If radiation is added to the convective cooling, the observed and theoretical temperature decays can be made to agree by using an emissivity of 0.85 for the

motor surface.

Early formulations of the model using conduction only were found not to dissipate heat rapidly enough using reasonable values of the thermal parameters to correspond with the data, so the formulation was changed to include radiation out the nozzle. With the full T^4 radiation law, the model was found to achieve reasonable temperatures with reasonable times and parameters, showing that radiation from the nozzle may be an important physical mechanism for dissipating the heat remaining immediately following firing. For this radiative heat transfer, the surroundings were taken to be at freezing, 273K, while the initial temperature of the interior was taken at 3600K.

In summary, the final form of the thermal model was one-dimensional in the radial dimension and time dependent using a step function initial temperature profile, four kinds of material (steel, liner, NBR and char), forced (linear) convective cooling of the surface with an empirically determined transfer coefficient, and radiative cooling of the interior.

4. Intercomparison between data and models: unknown parameter estimation

The intercomparison between the data and the models has been only touched on in this work. This is in part because much of the information of interest has been shown to be most evident in the early part of the cooling cycle, which is strongly affected by the injection of the carbon-dioxide fire suppressant. A detailed model of the early cooling would require a description of the amount of carbon dioxide used and its rate of injection. On the other hand, enough of an intercomparison has been made that the approach seems to be feasible, in that some parameters of the observations can be made to agree with model results for reasonable choices of the model parameters.

As discussed above, it was found necessary to formulate a model with the full T^4 variation of heat flux with temperature which corresponds to radiative heat transfer. With this term, the model became inherently nonlinear. The variation of peak temperature with char thickness was expected to reflect this non-linearity. It was therefore a pleasant surprise when the numerical experiments showed that the peak surface temperatures during the cooldown period varied linearly with the thickness of the char layer for both the 0.1 inch thick insulation layer and the 0.5 inch thick insulation layer. In addition, a two point test with initial temperatures of 2000K and 3600K showed that peak surface temperature was nearly proportional to initial temperature.

In contrast with the peak temperature estimates, the time estimates to peak temperature are smaller in the model results than in

the data by as much as a factor of four. It is also apparent that the early minutes following firing, the time during which the dynamic range of the measurements was small due to the imager scale chosen, are the most important for obtaining accurate heating values in the thin insulation areas. For the thick insulation areas, the discrepancies in time can be related to the insulation thickness by using a factor, the square of the ratio of actual insulation thickness to modeled insulation thickness, based on the conductive time constant for the insulation. A strict application of the square of the thickness ratio is not justified, for the peak of the thin insulation model results, 80 seconds for 0.1 inch thickness, should scale to 25 times that, or 2000 seconds, for the thick insulation. The model results for the thick insulation peak at only 1100 or 1200 seconds rather than 2000 seconds. For the thin insulation areas, an additional consideration is the response of the motor to the two thermal inputs, heating followed by cooling. Ancillary analytic and numerical modeling showed that a pattern of heating followed by cooling produces a later peak than a single stimulus and that the late cooling curve corresponds to the net heat applied. In order to calculate this effect in the motor, information is required describing the cooling event, such as the amount of carbon dioxide which was applied to the motor and the time of application. In order to verify such corrections to the model in the forward and center segments, data defining the peak temperatures are required during the time period of the data blackout. In addition, the noise level for the data early in the test is high because of the temperature range chosen. This combination of circumstances motivated the dropping of explicit modeling of the carbon dioxide cooling event.

Following the temperature peak at any location, a long period of cooling occurs. If the assumption of one-dimensionality holds during this period, which corresponds to many through skin characteristic times, the cooling should be exponential, with the characteristic time for the curve being related to the heat transfer coefficient between the motor surface and the environment. Conditions were particularly favorable for an exponential cooldown on the day of the test, for the sky was overcast and a fairly steady wind was blowing. These conditions promote a constant heat transfer coefficient because cooling is primarily conductive to the air, and solar radiation is greatly attenuated and diffused. The only difficulty in evaluating the coefficient from the data lies in the uncertainty of the value for the ambient temperature to assign to the relative image data. In order to estimate this ambient temperature, a series of graphs were made from the late data from Station 9, which appears to possess the best exponential late cooling curve in the data set. The results are shown in Figure 4.1, where the natural logarithm of the temperature rise is plotted as a function of elapsed time for each

of a sequence of assumed ambient temperatures, spanning the range from the temperature of the reaction mass to 10 degrees C. colder than the reaction mass. This range was considered to span the correct value from other considerations. Two curves were fitted to the data following the log transformation, a parabola and a straight line. The coefficient of the second order term of the parabola and the slope of the straight line curve were noted and are shown in Table 4.1 along with the resulting e-folding time constant corresponding to each curve. The curvature coefficient, rather than passing through a clear zero and changing sign, appears to preserve its sign and simply continue to reduce its magnitude as the offset temperature increases. The slope of the straight line obtained with a first order fit, when expressed as a characteristic time, adds a roughly constant amount (about 900 seconds) for each 2 degree increment in the offset.

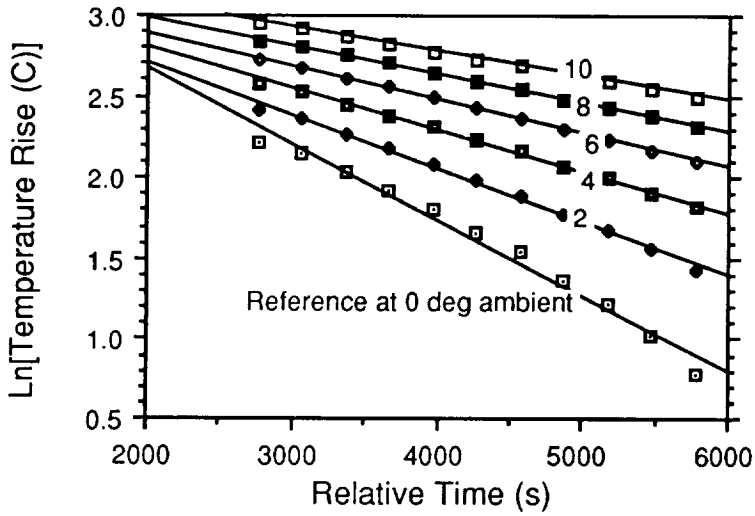

Figure 4.1. Logarithmically transformed cooling curves used to search for the ambient temperature value. The curves are extracted from the cooling segment of the time series data for Station 9.

Table 4.1. Parameters of the cooling curves obtained from the Station 9 data under the assumption of different ambient temperatures.

Temperature Offset (C)	Slope	Curvature	R-squared	Characteristic Time (s)
0	-1.7 E-4	-7.4 E-8	.999	2134 s
2	-8.0 E-5	-2.9 E-8	1.000	3058 s
4	-1.4 E-4	-1.3 E-8	1.000	3947 s
6	-1.6 E-4	-6.1 E-9	.999	4820 s
8	-1.6 E-4	-2.4 E-9	.999	5687 s
10	-1.5 E-4	-3.6 E-10	.999	6548 s

The correlation coefficient for the fits is between 1.0 and 0.999 for the three greatest offsets, indicating that all these lines fit the data well. The procedure, then, provides a lower value for the offset of ambient temperature from the reference temperature, but does not give a clear indication of an upper limit. Because other indications for the ambient temperature produced values of about 5 degrees below the reference, the value of 4800 seconds for the time constant, close to the 4820 seconds obtained from the 6 degree offset, was used for the model work. This value resulted in a total heat transfer coefficient of 9.1 $W/(m^2-K)$. Theoretical agreement is obtained by using the formula for forced convection in Carslaw and Jaeger [Eq. I(6)] with a wind speed of 20 mph and the formula for radiant heat flux in Carslaw and Jaeger [Eq. I.9(11)] using an emissivity estimate of 0.85. With these values, the calculated heat transfer coefficient is 9.20 $W/(m^2-K)$, and the radiant transfer accounts for 43% of the total. While the close numerical agreement is partly the result of a fortuitous choice of parameters in the equations, the measured value agrees in general with theoretical formulas, and the substantial contribution of radiant heat to total heat transfer is strongly indicated by the calculation.

The very long time behavior of the model contains an artifact, which is expressed as a lowering of temperature below the ambient temperature at long times. For example, at a time of 3 hours 20 minutes following ignition, the model shows a surface temperature of 261K, 12 degrees below ambient. An examination of the flux within the model shows that the steel portion is acting as a distributed heat sink, causing the lowered surface temperature. This response is non-physical. The value of the artificial flux is small with respect to fluxes during the period of interest, so it was permitted to remain, as it is not considered to affect any of the results or conclusions of this study.

5. Discussion

The first experiment run with the model, once parameters had been chosen, was to keep the grid and all parameters and boundary conditions fixed while permitting an increasing number of the insulation elements to become char and attain an initial temperature of 3600 K. This process models the increase of ablation depth which occurs on successively longer exposure of the insulation to the hot gasses. The resulting temperature evolution at the viewed surface is shown in Fig. 5.1a for the 0.1 inch thick insulation and Fig. 5.1b for the 0.5 inch insulation. The peak temperatures and times to peak temperature for the model are shown in Table 5.1. It is readily apparent that the peak temperatures are sensitive to the depth of the char layer. This is not surprising, for the model formulation is such that thicker char layers introduced correspondingly greater

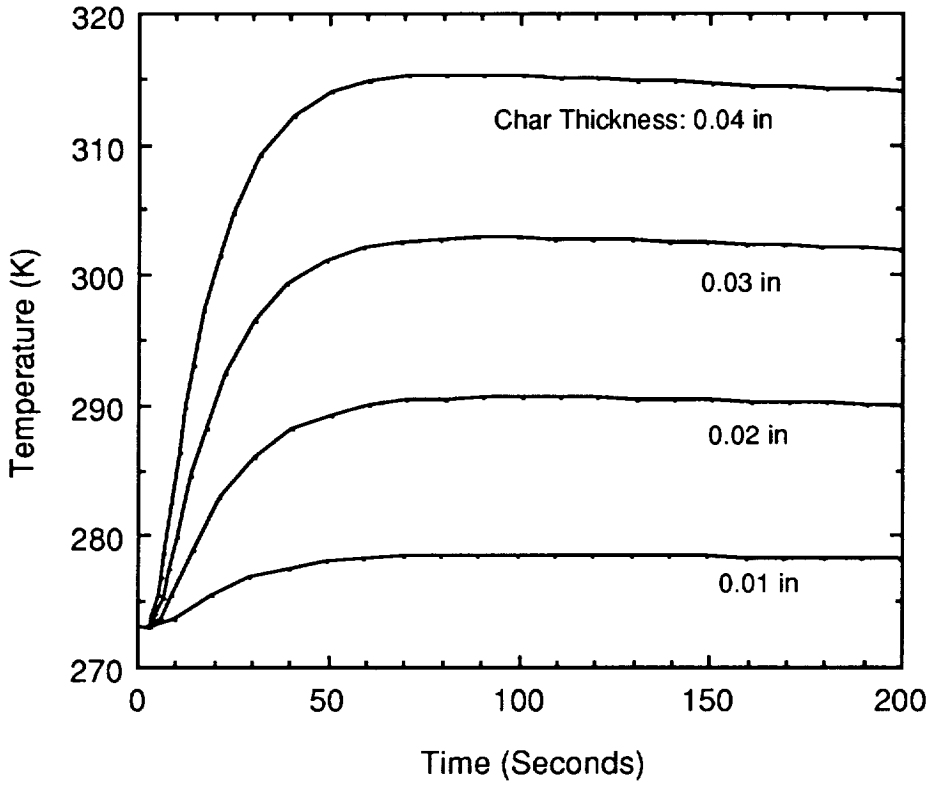

Figure 5.1a. Model results for an initial insulation thickness of 0.1 inches. Model parameters were chosen to represent a thin insulation segment of the Shuttle Solid Rocket Motor.

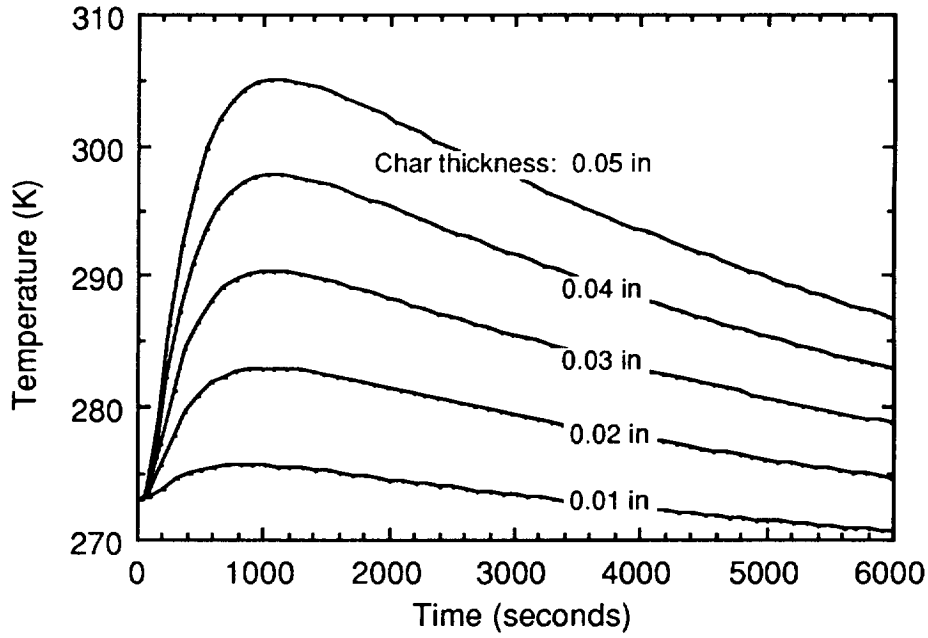

Figure 5.1b. Model results for an initial insulation thickness of 0.5 inches. Model parameters were chosen to represent a moderately thick insulation section of the Shuttle Solid Rocket Motor.

Table 5.1. Model output characteristics for varying combinations of char thickness and insulation thickness. Model parameters were chosen to represent the Shuttle Solid Rocket Motor.

Thickness of Remaining Insulation (in)	Thickness of hot char layer (in)	Number of hot nodes	Maximum temperature Rise (C)	Time of temperature maximum (s)
0.06	0.04	4	42.2	80-90
0.07	0.03	3	29.8	89-99
0.08	0.02	2	17.6	91-101
0.09	0.01	1	5.5	89-99
0.45	0.05	5	32.0	1055-1155
0.46	0.04	4	24.8	1039-1139
0.47	0.03	3	17.3	985-1085
0.48	0.02	2	9.9	987-1087
0.49	0.01	1	2.6	814-914

amounts of heat in excess of that contained at ambient temperature into the model. The effect is similar to that found with elevated initial temperatures. A plot of peak temperature versus char thickness, Fig. 5.2, shows that the relationship between the two is very linear, with a zero point of about one half of a model element. The correspondence between char thickness and heat input accounts for the one-half element discrepancy, for the model interpolation of the initial step temperature distribution includes a linear temperature distribution in the innermost char element, which has a temperature of 3600 C. on one side and 0 C. on the other side. Thus, this element

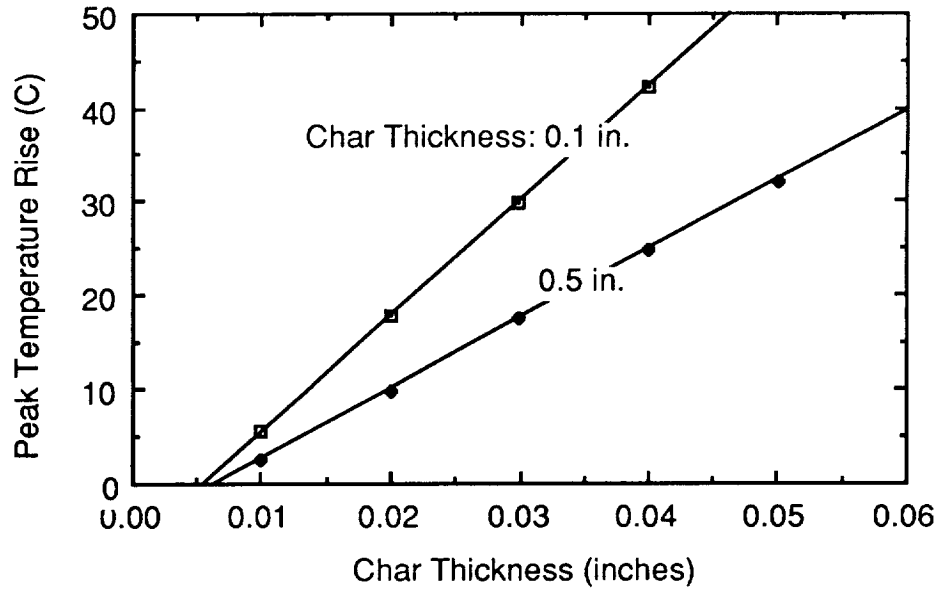

Figure 5.2. Model values of peak temperature rise as a function of char thickness. The two curves are for different initial insulation thicknesses. Model parameters have been chosen to represent the Shuttle Solid Rocket Motor.

contains only half the heat of the rest of the elements. What is remarkable is that the linearity is preserved despite the nonlinear radiation dominance of heat loss at early times. For the two cases studied, having insulation thicknesses of .1 inches or .5 inches, the slope of the peak temperature vs. char thickness line varies from 1223 to 737 C./inch of char, the ratio of slopes being 0.603. This is somewhat smaller than the ratios of total heat capacity in the two cases, 0.702, which would be expected by simply distributing a fixed percentage of heat from the initial conditions uniformly through the thickness of the material in the model. The difference can be ascribed to additional heat loss occurring in the thick insulation because its time to peak is greater than for the thin insulation.

The linear relation between peak temperature and char thickness in the model suggests that char thickness in the motor can be estimated if the amount of heat remaining in the case following burnout can be estimated. The amount of heat in the motor at a given position is well represented by the peak temperature at that position because, with the exception of the thick insulation in the aft portion of the motor, the steel case accounts for the preponderance of the heat capacity, and the inner insulation and char have come into thermal equilibrium with the case at the time of peak temperature. The amounts of heat measured at varying positions are not strictly comparable, because the the peak temperatures occur at different times for different parts of the motor. To bring the estimates into parity, it is necessary to express the heat amounts at a common time, such as right after burnout. To do this, allowance must be made for the different times of exposure to the atmosphere. Fortunately, the rate of cooling can be estimated from the long-time behavior of the cooling curves. Once this is known, if ablation/erosion has been minimal, the remaining char thickness can be calculated from a formula (Eq. 5.1) which requires only the original insulation thickness, the peak

$$D_3^{(n+1)} = \frac{T_p(C_1D_1 + C_2D_I)}{3600 f_1 C_3 \exp\left(\dfrac{-Rt_p}{C_1D_1 + C_2D_I + (C_3 - C_2)D_3^{(n)}}\right) - T_p(C_3 - C_2)} \qquad (5.1)$$

temperature rise and the time of the peak temperature rise. In this formula, subscripts 1,2 and 3 correspond to the steel skin, the insulation and the char respectively. T_p is the peak temperature which occurs at time t_p. The subscript I corresponds to the original insulation. D's are thicknesses and C's are volumetric heat capacities. R is the heat loss rate, and f_1 is the fraction of the total heat remaining following the initial radiation loss. The unknown in the equation is not entirely isolated on the left hand side, so the equa-

tion is solved iteratively, with the parenthetical values in the superscripts corresponding to estimate numbers. Iterations are continued until the difference between successive estimates is sufficiently small. A computer program, to perform this calculation has been written and is included, along with a more extensive derivation of Eq. 5.1, in the appendix. The results of the calculations for DM-9 are shown as Fig. 5.3 in comparison with the corresponding nominal

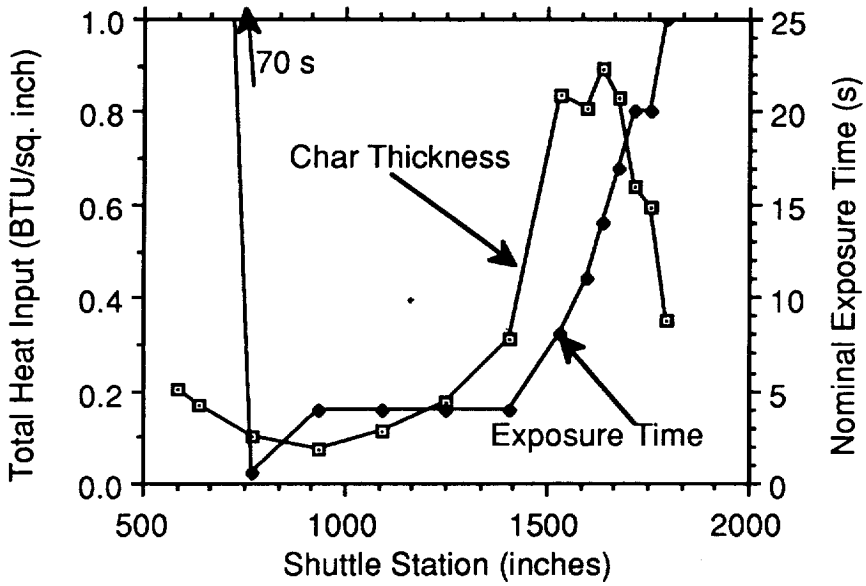

Figure 5.3 Estimates of relative char thickness, expressed as total heat, as a function of position on the Shuttle Solid Rocket Motor. The nominal time of exposure of the insulation to the flame is shown for comparison.

times of burnout as estimated in the Jones report. There is a general agreement of trends in the center of the motor, but the estimated exposure time at the ends of the motor is not nearly enough to agree with the nominal exposure time there. In the forward section, where the star grain is located, there are two factors which may account for this difference. First, the cooling by injection of carbon dioxide has not been taken into account in the model estimate. Second, after the star has burned out, the forward section becomes a "dead end", with no recently burned gasses necessarily passing it on their way to the nozzle. Thus, its interior temperature following burning may be lower than the remainder of the motor. At the back of the motor, the observed temperatures are once again much too low. This can be attributed partly to the cooling process following the burn and partly to the erosion of the insulation in the aft section of the motor. The remaining trend of total heat within each part of the motor, in regions away from the joint areas, does correspond qualitatively with the nominal times of exposure following burnout of each segment. In particular, the large increase in peak temperatures and

calculated char thickness in the aft section with respect to the rest of the motor corresponds with the early burnout in the aft section.

Another feature of the data is that the times before the peak temperature values vary substantially from the front to the back of the motor. As the time of exposure to hot gasses is much smaller than the time to the peak temperature, the evolution of the temperature curve follows a general curve which scales roughly as the square of

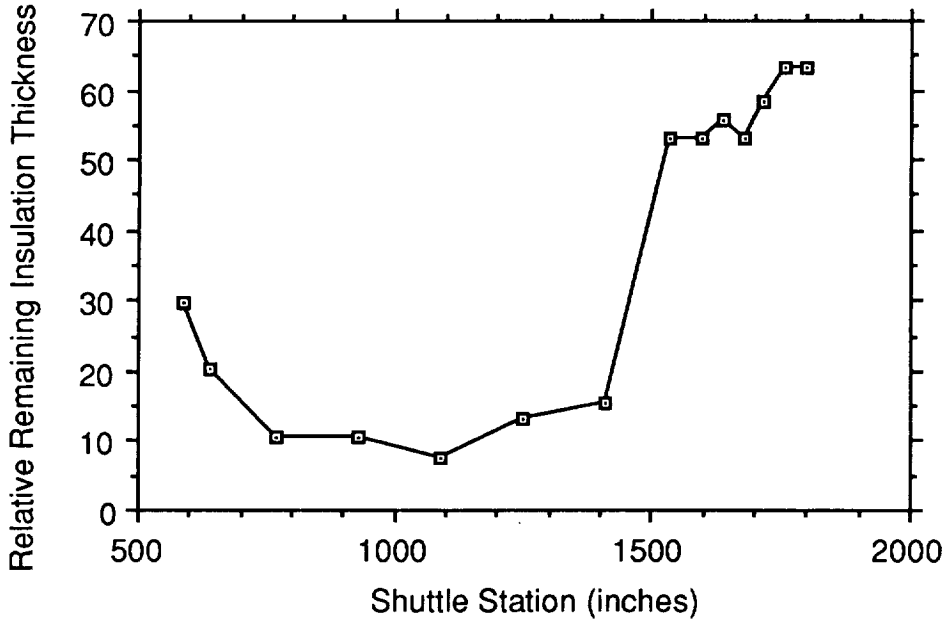

Figure 5.4. Estimates of relative thickness of remaining insulation from delay times of peak surface temperature following the burn in Test DM-9 of the Shuttle Solid Rocket Motor.

the thickness of NBR. The time to the peak temperature thus should provide an indication of the square of the thickness of the NBR remaining following the burn. A plot of the square root of the time to peak temperature versus position on the motor is given in Figure 5.4. This figure indicates that the least remaining insulation thickness is in the aft part of the forward segment and the center segments, with the forward part of the forward segment and the aft segment each having greater thickness of remaining insulation. To discriminate more closely between the thin insulation regions, more time resolution is required in the early frames of the data.

The temperature evolution in the thin insulation portion of the motor showed a more definite cooling event than in the thick insulation portion. An analytic model of heating followed by cooling was constructed to examine if this behavior was consistent with the scenario of brief heating followed by a longer period of cooling, the differences in response being primarily associated with the length of exposure time to the heating and the depth of the remaining insulation. The model included a heating and cooling pulse at the surface

of a semi-infinite insulation layer with thickness being examined by solving at different depths in the insulation. The early peak representing the difference between exposure heating and net heating vanished rapidly with insulation thickness, and was substantially gone at 0.3 inches, in agreement with the data. For thicker insulation, the response due to the total pulse became indistinguishable from that due to a single pulse carrying the same net amount of heat, in agreement with the single temperature maxima seen in the aft segments.

The only major characteristic in the data which is not qualitatively reproduced in the model is the secondary rise in temperature in the center sections. As this temperature rise is larger towards the back of the motor and as the aft section is the most likely source of the heat, it is apparent that the one-dimensional model is not strictly justified. There is heat exchanged between sections of the motor on the interior surface by either gas conduction or by radiation, which is not included in the models. To include this exchange, a model would need to be constructed consisting of a series of one-dimensional models attached by an appropriate transfer mechanism at one end. Short of this, heat transfer between motor segments by radiation or conduction in the motor interior is identified as being the greatest source of systematic error in the one-dimensional model.

6. Conclusion and recommendations

The Solid Motor Witness Test was conceived as a method of using infrared image data to evaluate some of the parameters of a solid rocket motor during a static firing. It has been shown that it is possible to extract meaningful and significant temperature data from the outside of the case of the motor during and subsequent to a firing. In doing this extraction, it has become evident that a given imager can be optimized either to capture extreme conditions in the event of a catastrophic failure or to document nominal operation during a more routine test, but not both. The data which were extracted were self consistent, but not corrected for emissivity, which was considered to be a constant over the motor. The justification for this assumption is that the paint on the surface was all fairly new and of the same type. If this were not true, a separate experiment would be required to obtain an emissivity map over the motor or to repaint the motor for the purpose of obtaining uniform, high emissivity. In some failure conditions short of pressure release, surface temperatures might become high enough to scorch the paint. The thermographic method would document such changes, but the ability to obtain self-consistent temperature data would be problematical in scorched areas. An additional requirement for obtaining data is that the motor be in the view of the imager. In the case of DM-9, the viewed area covered only between 20% and 30% of the motor surface.

The ability to use mirrors to increase the effective view of the imager by matching the aspect ratio of the motor more closely to that of the image was demonstrated. The use of an imager with a cooled detector requiring filling at two-hour intervals, while inconvenient, was demonstrated to be practical for static firings. To obtain nearly complete coverage, two imagers mounted on opposite sides of the motor are recommended. During the firing itself, the intense emission from the flare was not a problem for the imager because the flare was kept outside the image and because the cooled mercury-cadmium-telluride detector used in the imager has a short recovery time from extreme saturation. However, the temperature measured during firing was compromised by reflections of the flare by objects in the field of view. The consistency of the data was achieved partly by the use of a reference target in the field of view to allow correction for short term drift in the data. To improve the correction further, it is recommend that two large reference targets maintained at different known temperatures be included in further measurements with direct measurements taken of their temperatures. These targets would establish a reference base temperature and a temperature scale marker which could be used to maintain the accuracy of image contrasts in subsequent processing steps. By large is meant that the targets subtend at least 5 IFOV's in each of their two image directions. This can be accomplished by using large targets near the motor or smaller targets near the imager.

A physical model has been constructed which permits substantial data interpretation to be done using a substantially simplified approach. It reduces the heat flow in the motor case to one dimension so that the temperatures viewed on the outside of the motor result from heat inputs and material properties in the case directly inside of the viewed portion of the case rather than being influenced by adjacent segments. The physical justification for this simplification is the relative closeness of the inside of the motor to the surface compared with the large diameter and length of the motor.

Numerically, the reduction to one dimension greatly simplifies the formulation of a model by reducing the general problem of formulating a three-dimensional model of the entire motor to the formulation of a series on one-dimensional models at only the points for which temperature data are available. The complexity of the modeling effort is thus substantially reduced accompanied by a substantial improvement in the verifiability of the model. One advantage is that the model was formulated with much higher resolution than a full-motor model. The model simplicity was limited, however, by the nonlinearity imposed by radiative heat exchange which was found necessary to describe the initial cooling from the incandescent initial temperatures. The cooling used to extinguish the residual burning within the motor for the static test was not included in the model.

An analytic model to examine the effects of cooling indicated that this omission was relatively insignificant in the aft motor segment, where the insulation is thick and exposure times are long. The primary effect is to change the amplitude of the response to be that associated with net heat input rather than that associated with the burning only. In the forward and center segments, a residual heating spike was seen to propagate to the outer skin, the height of the spike depending on the thickness of the insulation. After several tens of minutes, the model failed to calculate an observed secondary heating in the central motor segments, the temperature rise increasing in the aft direction. This heating is attributed to conductive or radiative exchange between center and aft segments, the aft segments remaining considerably warmer than the remainder of the motor at this time.

The DM-9 test suffered a primary failure of a portion of the nozzle structure located in the interior of the motor. There was no indication of this failure apparent in the thermal data. Examination of the location of the failure suggested that no thermal indication would be expected of the failure due to the extremely long conductive path between the failed part and the viewed motor surface.

Of the motor parameters of primary interest, the results show that the interior temperature at burnout is difficult to estimate from the exterior temperature patterns. On the other hand, the exposure time, related to the time of burnout, and the thickness or remaining insulation are reasonably correlated with parameters of the thermal cooldown data. In particular, the anomalies in exposure time associated with the fin pattern in the forward segment are expressed as thermal patterns on the motor surface. Analysis of thermal data may be of use to motor designers interested in these properties, which are obtained at present through point sampling methods only. The data may be used to interpolate between or reduce the number of points at which samples of char thickness and remaining insulation thickness need to be taken during the evaluation of a motor test.

7. Acknowledgements

The work reported here was supported financially under Task Assignment 3 of NASA Contract NAS1-18347 between NASA Langley Research Center and the College of William and Mary. Field work was done at the Wasatch Facility of Thiokol, Inc. Brigham City, Utah. In particular, Mr. Tim Eden in the R&D Laboratory and Mr. Fred Wilson of the Photography Department provided both access and support which were necessary to obtain the data. Other Thiokol personnel in the

above departments, Quality Assurance and Production facilities also provided excellent cooperation and support. Besides colleagues in the Instrument Research Division at NASA Langley Research Center, support and help were obtained from the Structures Division and from NASA Marshall Space Flight Center. Helpful review comments were obtained from D. Garecht, D Nisonger and E. Mathias of Thiokol, Inc. and S. Ravzi of Marshall Space Flight Center.

Appendix: Program CharThick

This program was written to implement evaluation of Equation 5.1, which uses easily evaluated parameters from a temperature record to make an estimate of the thickness of the char layer in a solid rocket motor. It is based on equating two estimates of the heat remaining in the motor at the time of observation of the temperature peak and expressing the resulting formulas in terms of known quantities as far as possible. The geometry is considered locally to be represented by three slabs, representing the steel case, the remaining insulation and the char layer referred to with subscripts 1,2 and 3, respectively. The material properties consist of slab thicknesses, denoted by D, and volumetric heat capacities, denoted by C. The heat estimates are Q_{init}, the heat in the char layer a few seconds following the end of burning (time = 0), after the incandescent radiation has finished dumping large amounts of heat out the nozzle, and Q_{obs}, the amount of heat, by that time having uniform temperature, T_p, through the thickness of the three slabs, observed at the time of peak temperature (t_p). Before equality of the two heats can be asserted, allowance must be made for the cooling of the motor between the times of 0 and t_p. A crude allowance is made by assuming that the exponential cooling rate, R, found directly from the later data can be applied backwards to zero time. Thus, the basic equation is

$$Q_{init}\exp(-Rt_p/C_T) = Q_{obs}.$$

in which C_T is the total heat capacity of the entire section. Now $Q_i = T_iC_iD_i$, where i represents any subscript. At time zero, all the heat is located in the char layer, and it can be accounted for as $Q_{init} = T_3C_3D_3$. D_3 is the quantity sought, and C_3 is known. T_3 is the temperature of the char following the burn, and is expressed as 3600 f_1, where the interior reaction temperature is taken as 3600C and f_1 is the remaining fraction of heat at zero time, estimated as 0.828 from numerical model experiments. For the right hand side, $Q_{obs} = C_TT_p$. The total heat capacity is $C_T = C_1D_1 + C_2D_2 + C_3D_3$. In this expression, D_2 and D are both unknown. The assumption of no erosion is made at this point to assert that $D_2 + D_3 = D_I$, the initial insulation thickness, which is known. Thus, one can express the total heat capacity as $C_T = C_1D_1 + C_2D_I + (C_3 - C_2)D_3$. When this is done, all of the D_3 terms can be grouped except the one in the denominator of the exponential, which has a fairly small effect because of the preponderance of the steel case in determining total heat capacity over much of the motor. The equation cannot be quite solved analytically, but if an initial estimate is made for D_3 by ignoring the D_3 value in the exponential, and then successive estimates are made by using the previous estimates in the exponential, the iteration con-

verges quickly to a consistent value of D_3. This is represented as Eq. 5.1, and the following program implements the iteration scheme in FORTRAN. In this program, the values for known material and rate constants are given directly in their respective declarations, and they may be changed to represent other situations.

```
C     Program CharThick.For
C     Version CSW1.0 - Started 15 December 1989
C     This program evaluates a simple recursive model to calculate
C     the thickness of the char layer in a solid rocket motor from the
C     maximum temperature and time to reach maximum temperature in a
C     static test.  The formula is
C
C              Tp*(C1*D1 + C2*Di)
C       D3 = ----------------------------------------------
C          T0*f1*C3*exp[-R'*Tau / sum(Cj*Dj)] - Tp*(C3-C2)
C
C    As the unknown, D3 is also part of the sum in the exponential, it
C    is evaluated recursively starting with D3 = 0 until D3 is stable
C    under iteration.
      Implicit none
C     Formula Variables:
      Real*4 T0 /3600./      ! Initial Temperature of interior (K)
      Real*4 Tp              ! Observed peak temperature
      Real*4 f1 /.828/       ! Fraction of initial heat remaining
C                            !   after initial radiative cooling
      Real*4 R  /9.1/        ! Heat loss rate to environment in
C                            !      (W/(m**2-K)
      Real*4 alpha /.762/    ! Ratio of average to peak temperature
C                            ! over time to peak temperature
      Real*4 Rprime          ! loss rate to environment
      Real*4 C1 /3.60e6/     ! Volumetric heat capacity of
C                            ! steel (W/(m**3-K)
     Real*4 C2 /2.05e6/      !     "       "      "      " insulation
      Real*4 C3 /0.72e6/     !     "       "      "      "   char
      Real*4 D1 /1.24e-2/    ! Thickness of the steel skin (m)
      Real*4 D3              ! Thickness of the char layer  (m)
      Real*4 Di              ! Initial thickness of the insulation
C                            !      in (m)
      Real*4 tau             ! Time of peak temperature
      Real*4 epsilon /.00001/! Incremental variation between
C                            ! iterations
C                            !threshold for calculation termination
      Real*4 Num,Den,Arg     ! Intermediate Calculation variables
      Real*4 Ratio           ! Trial variation between interations
      Real*4 OldD3           ! Result of previous iteration
```

```
      Integer*4 i              ! Iteration Counter
      Integer*4 MaxI /100/     ! Run-away iteration stop
C
C     General Initialization
C
      RPrime = R * alpha
C
C     Get Information and initialize calculation
C
  100 Continue
      OldD3 = 0
      Print *, 'Program CharThick - Char thickness estimation.'
      Print *, 'Enter negative insulation thickness to stop.'
      Write (*,'($''     Enter insulation thickness (m): '')')
      Accept *, Di
      If (Di .lt. 0) Goto 200
      Write (*,'($''    Enter peak temperature rise (K): '')')
      Accept *, Tp
      Write (*,'($'' Enter time of peak temperature (s): '')')
      Accept *, Tau
C
C     Perform Calculation
C
      i=0
      Ratio = 1
      D3 = 0.
      OldD3 = 0.
      Do while (Abs(Ratio) .gt. epsilon)
         i = i + 1
         If (I .gt. MaxI) then
            Print *,' Maximum iteration count exceeded.'
            Print *,' Present D3 is: ',D3
            Print *,'    Last D3 is: ',OldD3
            GoTo 100
         End if
         OldD3 = D3
C  If documentation of parameter values is desired, remove
C     the comment status of the following statmements.
C               Print *,' Tp = ',Tp
C               Print *,' C1 = ',C1
C               Print *,' C2 = ',C2
C               Print *,' D1 = ',D1
C               Print *,' Di = ',Di
C               Print *,' RPrime = ',Rprime
C               Print *,' Tau = ',Tau
```

```
C                Print *,' T0 = ', T0
C                Print *,' f1 = ', f1
         Num = Tp*(C1*D1 + C2*Di)
         arg = (-RPrime*Tau)/((C1*D1 + C2*Di) + (C3-C2)*OldD3)
C                Print *,'Num = ', num
C                Print *,'Arg =', arg
         Den = T0*f1*C3*exp(arg) - Tp*(C3-C2)
C                Print *,'Den = ',Den
         D3  = Num/Den
         Ratio = (D3 - OldD3)/D3
      End do
C
C     Report Results
C
      Print *, i,' iterations. D3 = ',D3
      GoTo 100    ! Back to get information for next calculation
  200 Stop 'Normal end to program CharThick'
      End
```

References:

Carslaw, H. S. and J. C. Jaeger, Conduction of Heat in Solids, Second Edition, 510pp., Oxford University Press, Oxford, U.K., 1959.

Shapiro, Arthur B., TOPAZ2D -- A Two-Dimensional Finite Element Code for Heat Transfer Analysis, Electrostatic, and Magnetostatic Problems, 110 pp., UCID-20824, Lawrence Livermore National Laboratory, University of California, Livermore, California, 94550, July, 1986.

Welch, C., and T. J. Eden,"Numerically enhanced thermal inspection of shuttle solid rocket motor inhibitor/liner/fuel bondline," Review of Progress in Quantitative Nondestructive Evaluation, Vol. 8b, D. O. Thompson and D. E. Chimenti, eds., pp. 2027-2034 , Plenum Publishing Corporation, 1989.

representative test points on the rocket motor surface as the motor cooled

NASA
National Aeronautics and Space Administration

Report Documentation Page

1. Report No.	2. Government Accession No.	3. Recipient's Catalog No.
NASA CR-4415		

4. Title and Subtitle	5. Report Date
Solid Rocket Motor Witness Test	December 1991
	6. Performing Organization Code

7. Author(s)	8. Performing Organization Report No.
Christopher S. Welch	
	10. Work Unit No. 505-63-01-17

9. Performing Organization Name and Address	11. Contract or Grant No.
The College of William and Mary Department of Physics Williamsburg, VA 23185	NAS1-18347
	13. Type of Report and Period Covered
12. Sponsoring Agency Name and Address	Contractor Report
National Aeronautics and Space Administration Langley Research Center Hampton, VA 23665-5225	14. Sponsoring Agency Code

15. Supplementary Notes

Langley Technical Monitor: W. P. Winfree
Final Report - Task 3

16. Abstract

The Solid Rocket Motor Witness Test was undertaken to examine the potential for using thermal infrared imagery as a tool for monitoring static tests of solid rocket motors. The project consisted of several parts: data acquisition, data analysis, and interpretation. For data acquisition, thermal infrared data were obtained of the DM-9 test of the Space Shuttle Solid Rocket Motor on December 23, 1987, at Thiokol, Inc. test facility near Brigham City, Utah. The data analysis portion consisted of processing the video tapes of the test to produce values of temperature at representative test points on the rocket motor surface as the motor cooled down following the test. Interpretation included formulation of a numerical model and evaluation of some of the conditions of the motor which could be extracted from the data. These parameters included estimates of the insulation remaining following the tests and the thickness of the charred layer of insulation at the end of the test. Also visible was a temperature signature of the star grain pattern in the forward motor segment.

17. Key Words (Suggested by Author(s))	18. Distribution Statement
space shuttle booster solid rocket motor insulation infrared thermography temperature measurement solid rocket static test	Unclassified - Unlimited Subject Category 20

19. Security Classif. (of this report)	20. Security Classif. (of this page)	21. No. of pages	22. Price
Unclassified	Unclassified	40	A03

NASA FORM 1626 OCT 86

NASA-Langley, 1991

For sale by the National Technical Information Service, Springfield, Virginia 22161-2171